Supporting information:

Preparation of Fe-N-C Catalysts with FeN_x (x=1, 3, 4) Active Sites and Comparison of Their Activities for Oxygen Reduction Reaction and Performances in Proton Exchange Membrane Fuel Cell

*Yongcheng Li,[1] Xiaofang Liu,[1] Lirong Zheng,[2] Jiaxiang Shang,[*1] Xin Wan,[1] Riming Hu,[1] Xu Guo,[1] Song Hong[c] and Jianglan Shui[*1]*

[1]School of Materials Science and Engineering, Beihang University, No. 37 Xueyuan Road, Beijing 100083, China
[2]Beijing Synchrotron Radiation Facility, Institute of High Energy Physics, Chinese Academy of Sciences, No. 19 Yuquan Road, Beijing 100049, China

[3]State Key Laboratory of Chemical Resources Engineering Beijing Key Laboratory of Electrochemical Process and Technology for Materials, Beijing 10029, China

E-mail: shangjx@buaa.edu.cn; shuijianglan@buaa.edu.cn

Experimental Section

1. Materials

Chemicals

Zinc nitrate hexahydrate ($Zn(NO_3)_2.6H_2O$, 99%), zinc oxide (ZnO) and 2-Methylimidazole (2MIm) were purchased from Sinopharm Chemical Reagent. Pt/C(20 wt%) catalyst was purchased from BASF. Ferric chloride ($FeCl_3 \cdot 6H_2O$, 99%) was purchased from Xilong Scientific Co., Ltd. Carbon black (BP) were purchased from Aladdin Industrial Corporation. All reagents are of analytical grade and used as received without further purification.

Preparation of ZIF-8 by liquid-phase synthesis method

ZIF-8 NPs with a size around 100 nm were prepared following a reported liquid-phase synthesis method with a little modification.[1] $Zn(NO_3)_2 \cdot 6H_2O$ (2.94 g) was dissolved in 100 mL methanol. 2MIm (3.24 g) was dissolved in another 100 mL methanol. Then, the 2MIm solution was poured into the $Zn(NO_3)_2 \cdot 6H_2O$ solution. The mixture was stirred for 2.5 hours at room temperature (20 °C). The obtained precipitate was collected by centrifugation, washed three times with methanol, and finally dried in vacuum at 60 °C overnight.

Preparation of ZIF-8 by solid-phase synthesis method

2MIm (1.707 g) and ZnO (0.638 g) were uniformly mixed and sealed in an autoclave in Ar atmosphere. The mixture was heat treated at 220 °C for 18 hours in the autoclave. The obtained white crystals were ball-milled for 8 h with 6 mm stainless steel balls at 300 rpm under Ar protection.

Preparation of FeNC-300/500/1000 catalysts

ZIF-8 powder was placed in a ceramic boat and heated in a tube furnace at 1000 °C for 1 hour under flowing Ar gas. The obtained products were intermediate nitrogen doped carbon (denoted as N/C*). 80 mg N/C* was added into a three-neck flask (50 mL) containing DI water (80 mL) to form a homogeneous suspension by ultrasonication. $FeCl_3 \cdot 6H_2O$ (22.84 mg) was dissolved in DI water (4.56 mL) and dropwise added into the N/C* suspension. After stirring for 60 min at room temperature, the suspension was heated at 70 ºC for 8.5 h. The Fe^{3+} anchored N/C (Fe@N/C*) NPs, was thoroughly washed and collected by centrifugation, and then dried in a vacuum oven at 60

ºC for 5 hours. The catalysts FeNC-300, FeNC-500 and FeNC-1000 were obtained by heating Fe@N/C* at 300, 500 and 1000 °C under Ar atmosphere for 2 h, respectively.

Note: For accurate parallel comparison, the reference catalyst, i.e. nitrogen doped carbon (denoted as N/C), was also washed with DI water, dried and heat treated at 1000 °C for 2 h.

Preparation of catalysts Fe-C-300/500/1000

80 mg carbon black was added into a three-neck flask (50 mL) containing DI water (80 mL) to form a homogeneous suspension by ultrasonication. $FeCl_3 \cdot 6H_2O$ (22.84 mg) was dissolved in DI water (4.56 mL) and dropwise added into the carbon black suspension. After stirring for 60 min at room temperature, the suspension was heated at 70 ºC for 8.5 h. The Fe^{3+} anchored C (Fe@C), was thoroughly washed and collected by centrifugation, and then dried in a vacuum oven at 60 ºC for 5 hours. The catalysts Fe-C-300, Fe-C-500 and Fe-C-1000 were obtained by heating Fe@C at 300, 500 and 1000 °C under Ar atmosphere for 2 h, respectively.

Preparation of catalysts NC-300/500/1000

80 mg N/C* was added into a three-neck flask (50 mL) containing DI water (80 mL) to form a homogeneous suspension by ultrasonication. After stirring for 60 min at room temperature, the suspension was heated at 70 ºC for 8.5 h, and was thoroughly washed and collected by centrifugation, and then dried in a vacuum oven at 60 ºC for 5 h. The catalysts NC-300, NC-500 and NC-1000 were obtained by heating N/C* at 300, 500 and 1000 °C under Ar atmosphere for 2 h, respectively.

2. Electrochemical measurements

Half-cell tests

The oxygen reduction reaction (ORR) activities of the catalysts were measured by a rotating ring-disk electrode (RRDE, Pine Research Instrumentation, USA) technique with a three-electrode system in 0.5 M H_2SO_4 or 0.1 M KOH water solution at a rotating speed of 1600 rpm. Poisoning test was conducted by adding KSCN water solution (0.375 M, 2 mL) into O_2-saturated H_2SO_4 (0.5 M, 150 mL) during Chronoamperometric experiment at 0.50 V vs RHE. The reference electrode was a saturated calomel electrode (SCE) and the counter electrode was a carbon rod. All potentials measured in this work were converted to the reversible hydrogen electrode (RHE) scale.

The non-Pt catalyst ink was prepared by mixing 5 mg catalyst in a mixture of 10 μL Nafion alcohol solution (5 wt.%, Aldrich), 215 μL deionized water and 275 μL isopropanol, and then sonicating for 20 min to form a homogeneous catalyst ink. The catalyst ink was loaded on a glass carbon electrode with a loading of 0.4 mg cm^{-1}. The concentration of Pt/C(20%) ink was 0.5 mg mL^{-1}, and the Pt loading was 20 μg cm^{-2} on the glass carbon electrode.

The capacitive background of catalyst was obtained in Ar-purged electrolyte at a scan rate of 10 mV s^{-1}. Before each electrochemical measurement, the electrolyte solution was purged with O_2 for 30 min to achieve a O_2-saturated solution. 20 cycles of cyclic voltammetry were firstly applied on the electrode to make a stable polarization curves, then linear sweep voltammetry (LSV) was recorded. The oxygen reduction currents were obtained by subtracting the capacitive background measured in the Ar-saturated electrolyte. The ring potential was set at 1.25 V vs. RHE to oxidate H_2O_2.The stability tests were performed in O_2-saturated 0.5 M H_2SO_4 at 0.5 V vs. RHE.

The peroxide yield was calculated from the ring current (I_r) and the disk current (I_d) using the equation:

$$H_2O_2(\%) = 200 \times \frac{I_r}{I_r + 0.37 I_d} \quad \text{(S1)}$$

The electron transfer number in acid was computed by the equation:

$$n = \frac{4 I_d}{I_d + \frac{I_r}{0.37}} \quad \text{(S2)}$$

The collection efficiency of the Pt ring was 37%.

Proton exchange membrane fuel cell tests

The catalyst and Nafion solution (dry weight ratio of 1:1) were mixed in isopropanol/water (volume ratio of 1:1). The ink was sonicated and stirred to form a homogeneous catalyst ink. Afterwards, the ink was brushed onto a piece of 5 cm^2 carbon paper and dried in a vacuum oven at 80 ºC for 2 h. The cathode catalyst loading was 1 to 4 $mg \cdot cm^{-2}$ for non-Pt catalysts and 0.35 $mg \cdot cm^{-2}$ for Pt/C(20 wt%). The anode was the same Pt/C(20 wt%) electrode. Then the as-prepared anode and cathode were sandwiched in a piece of Nafion 211 membrane (DuPont®), which was hot-pressed at 130 ºC for 2 min under a pressure of 300 pounds cm^{-2} to obtain a membrane electrode assembly (MEA). The MEA performance was assessed in a fuel cell fixture controlled by a fuel cell test station (850e,

Scribner Associates Inc.). The fuel cell operation condition is: 80 °C, 100% humidified H_2 and O_2 with flow rates of 200 and 240 mL min^{-1}, respectively. The gauge pressures of H_2 and O_2 were 22 psig.

3. Characterization

The morphologies of the materials were characterized by scanning electron microscopy (SEM, JSM-7500F, JEOL) and scanning transmission electron microscopy (STEM, JEM-2100F, JEOL) equipped with an energy-dispersive X-ray spectroscope (EDS, X-Max-65T, Oxford) for collecting the elemental mapping of the catalysts. The images of single iron atoms were obtained by a high-angle annular dark-field scanning transmission electron microscopy (HAADF-STEM, FEI Titan Cubed Themis G2 300) operated at 200 kV. The crystal structure of the samples was characterized by X-ray diffractometer with Cu Kα irradiation (Rigaku D/max 2500). X-ray photoelectron spectroscopy (XPS) measurements were performed on ESCALAB 250Xi using Al Kα irradiation. Nitrogen adsorption–desorption isotherms were collected by the SSA-7000 system (bjbuilder Instruments) at 77.3 K. Inductively coupled plasma optical emission spectroscopy (ICP-OES) was conducted on the Optima-7000DV. The specific surface area was obtained using the Brunauer–Emmett–Teller (BET) method. X-ray absorption spectroscopy (XAS) was performed at room temperature on the 1W1B beamline at BSRF (Beijing Synchrotron Radiation Facility). The catalyst sample was prepared by pressing a disk (diameter 6 mm) with ~30 mg catalyst and paraffin binder. The reference sample of iron phthalocyanine was prepared by mixing with BN powder at a weight ratio of 1:6. Transmissive-mode Fe K-edge XAFS data were collected for all samples over a range of 6974-8110 eV, where a 100% Ar filled Lytle ion-chamber detector with Mn X-ray filters and soller slits were used. The monochromator energy was calibrated using a Fe foil. The XAFS data were analyzed using IFEFFIT[2]. Least-squares curve parameter fitting was performed to obtain the quantitative structural parameters around iron atoms, using the ARTEMIS module of IFEFFIT software packages. The XAFS raw data were background subtracted, normalized and Fourier transformed by standard procedures within the ATHENA program. The FeN_x (x=1, 3, 4) moiety models were built based on pyridinic N-based structures, which are widely used in many studies of M-N-C catalysts as shown in Figure S14.[3-5] To avoid artificial biases, all models were optimized by density functional theory (DFT) calculation. Thermogravimetric analysis (Netzsch STA449F3, Germany) were performed in air atmosphere at the temperature range of 20-850 °C with a heating rate of 10 °C min^{-1}.

4. DFT calculations

The computations were performed using the Vienna ab initio simulation package (VASP)[6, 7] in the framework of density functional theory (DFT). The projector augmented wave (PAW)[8] pseudopotential was adopted and the GGA exchangecorrelation function was described by Perdew Burke Ernzerhof (PBE).[9] The cutoff energy of the plane-waves was set to 500 eV. The Brillouin zone was sampled with a Monkhorst-Pack 3×3×1 *k*-point grid. The force convergence criterion for atomic relaxation was 0.01 eV $Å^{-1}$.

The formation energy (*Ef*) was calculated as:

$$E_f = E_{total} - \sum_x n_x \mu_x \quad \text{(S3)}$$

where E_{total} is the total energy of the Fe and N embedded systems, n_x is the number of C, N and Fe atom. μ_x refer to the chemical potential of a single atom derived from graphene, N_2 molecule and a single Fe atom in vacuum, respectively.

The adsorption energies of oxygen-containing intermediates on FeN_x (x=1~5) were calculated as follows:[10]

$$\Delta E_{O^*} = E_{O^*} - E_* - [E_{H_2O} - E_{H_2}] \quad \text{(S4)}$$

$$\Delta E_{OH^*} = E_{OH^*} - E_* - [E_{H_2O} - 1/2E_{H_2}] \quad \text{(S5)}$$

$$\Delta E_{OOH^*} = E_{OOH^*} - E_* - [2E_{H_2O} - 3/2E_{H_2}] \quad \text{(S6)}$$

where E_*, E_{O^*}, E_{OH^*}, and E_{OOH^*} stand for the total energies of catalyst substrate without and with the adsorption of O, OH and OOH, respectively. E_{H_2O} and E_{H_2} are the total energies of H_2O and H_2 molecules in gas phases, respectively. According to the formula, a more negative value of E_{ads} indicates a higher thermodynamic stability of the composite system. The adsorption free energies can be obtained by including the zero point energy (ZPE) energies and entropy (S) corrections in equation:

$$\Delta G = \Delta E_{ads} + \Delta ZPE - T\Delta S \quad \text{(S7)}$$

The ΔZPE and ΔS could be obtained from the calculation of vibrational frequencies for the adsorbed species. The entropies and vibrational frequencies of the species in gas phase were taken from NIST database.

As for oxygen reduction reaction (ORR) in acid electrolyte, the overall reaction scheme of the ORR can be written as:

$$O_2 + 4(H^+ + e^-) \rightarrow 2H_2O \quad (S8)$$

The ORR can be carried out by following four basic steps (S1-S4), which are commonly used to study the electrocatalysis of the ORR on various materials:

$$O_2(g) + {}^* + (H^+ + e^-) \rightarrow OOH^* \quad (S9)$$

$$OOH^* + H^+ + e^- \rightarrow O^* + H_2O(l) \quad (S10)$$

$$O^* + H^+ + e^- \rightarrow OH^* \quad (S11)$$

$$OH^* + H^+ + e^- \rightarrow H_2O(l) + {}^* \quad (S12)$$

where * stands for an active site on the base site, (l) and (g) refer to liquid and gas phases, respectively. O*, OH*, and OOH* are adsorbed intermediates.

The calculation of ORR free energy diagrams was performed according to the method proposed by Nørskov et al.[11] The free energy was calculated by the equation:

$$\Delta G = \Delta E + \Delta ZPE - T\Delta S \quad (S13)$$

where *ΔE* is the reaction energy change obtained from DFT calculations, *T* is the temperature (298.15K). The free energy of ($H^+ + e^-$) under standard conditions at pH=0 and U = 0 is taken to be 1/2 of H_2. The free energy of O_2 was obtained from the free energy change of the reaction $O_2 + 2H_2 = 2H_2O$ for which a free energy change is 4.92 eV at the temperature of 298.15 K and the pressure of 0.035 bar.[12, 13]

ZPE and *TS* of gas molecules and the ORR intermediates were listed in Supplementary Table S10. The ORR overpotentials (η) can be computed by the equations as follows:

$$\eta = max(\Delta G1, \Delta G2, \Delta G3, \Delta G4)/e + 1.23V \quad (S14)$$

5. Supplemental Figures and Tables

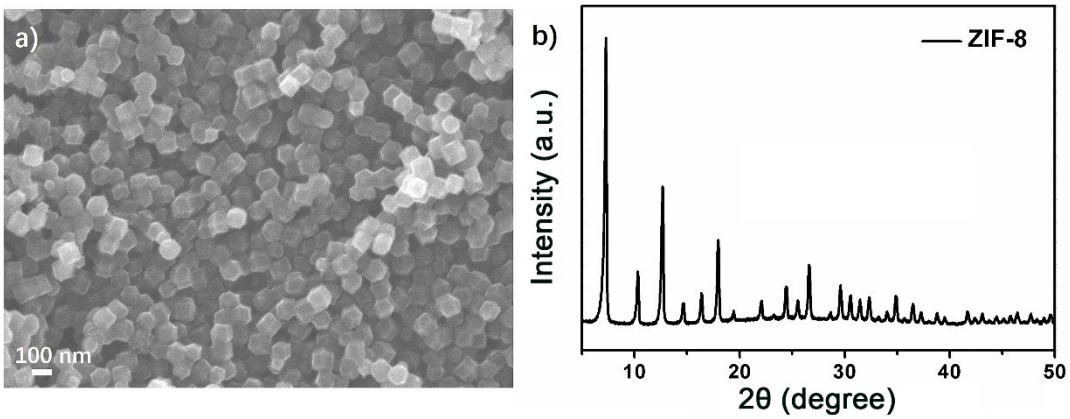

Figure S1. a) SEM image and b) XRD pattern of ZIF-8 NPs synthesized through a liquid-phase approach.

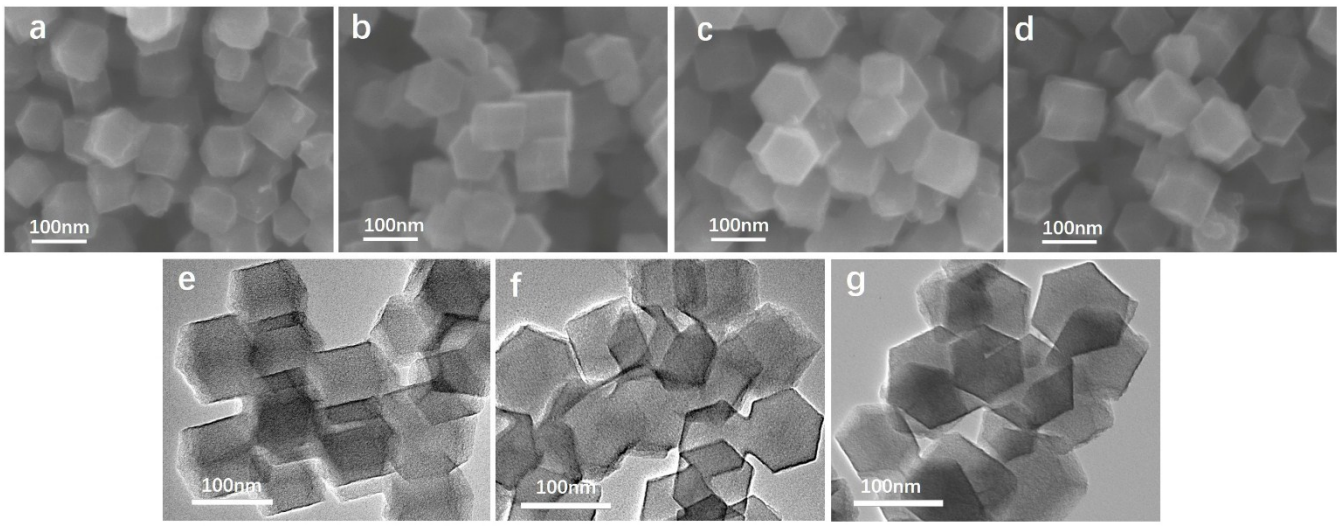

Figure S2. SEM images of a) N/C, b) FeNC-300, c) FeNC-500, d) FeNC-1000 and TEM image of e) FeNC-300, f) FeNC-500, g) FeNC-1000.

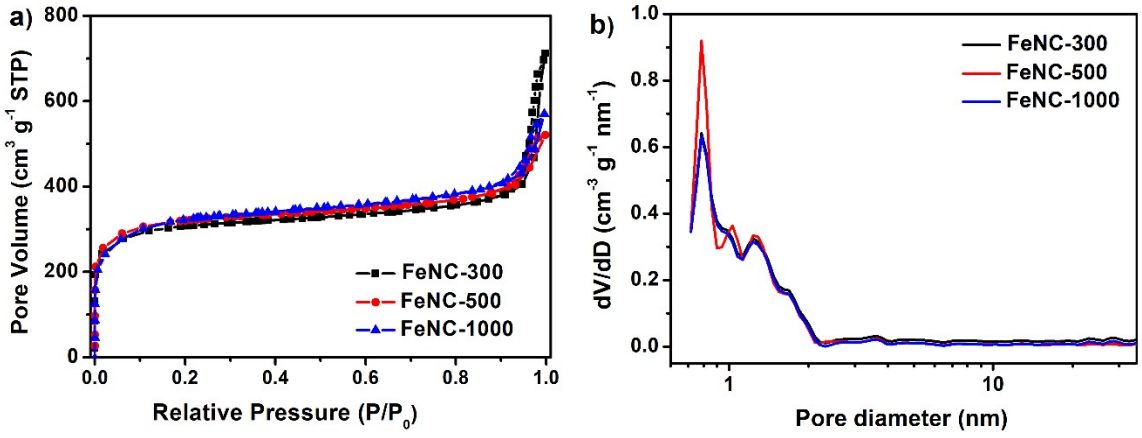

Figure S3. a) N_2 adsorption and desorption isotherms and b) pore size distribution of FeNC-300/500/1000.

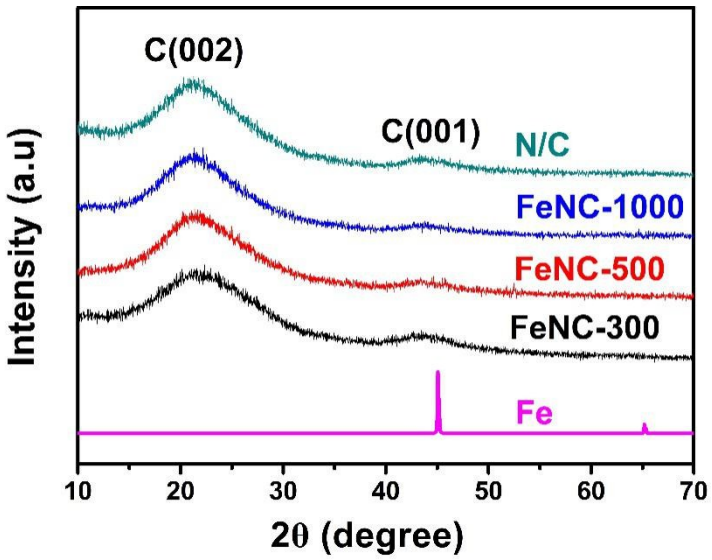

Figure S4. XRD patterns of N/C, FeNC-300, FeNC-500 and FeNC-1000.

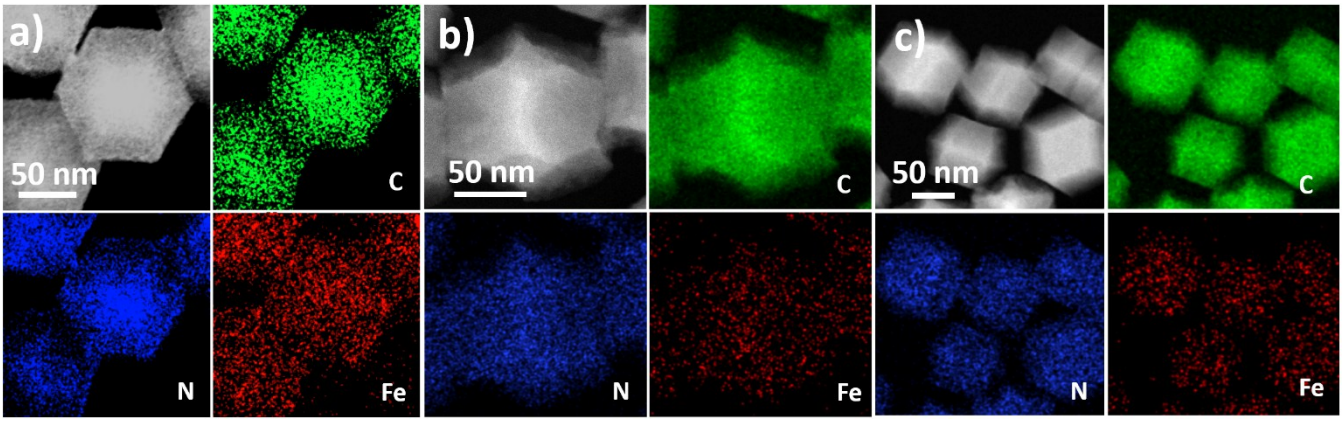

Figure S5. STEM image and corresponding elemental mappings of a) FeNC-300, b) FeNC-500 and c) FeNC-1000 nanoparticles.

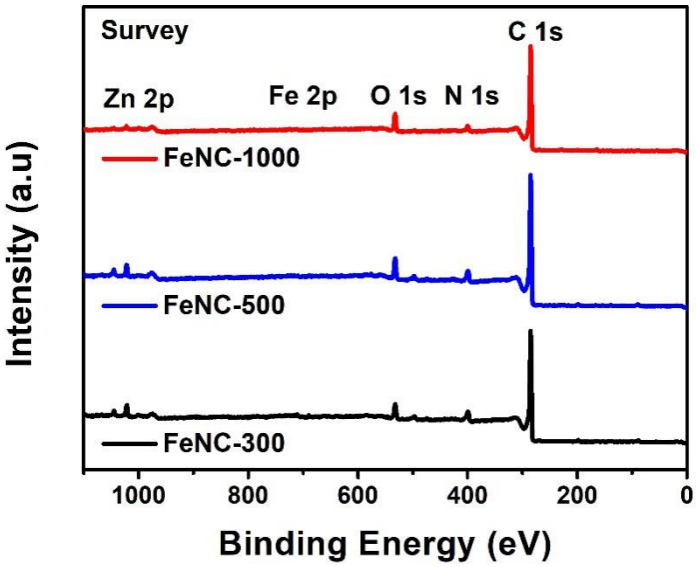

Figure S6. XPS survey of FeNC-300/500/1000.

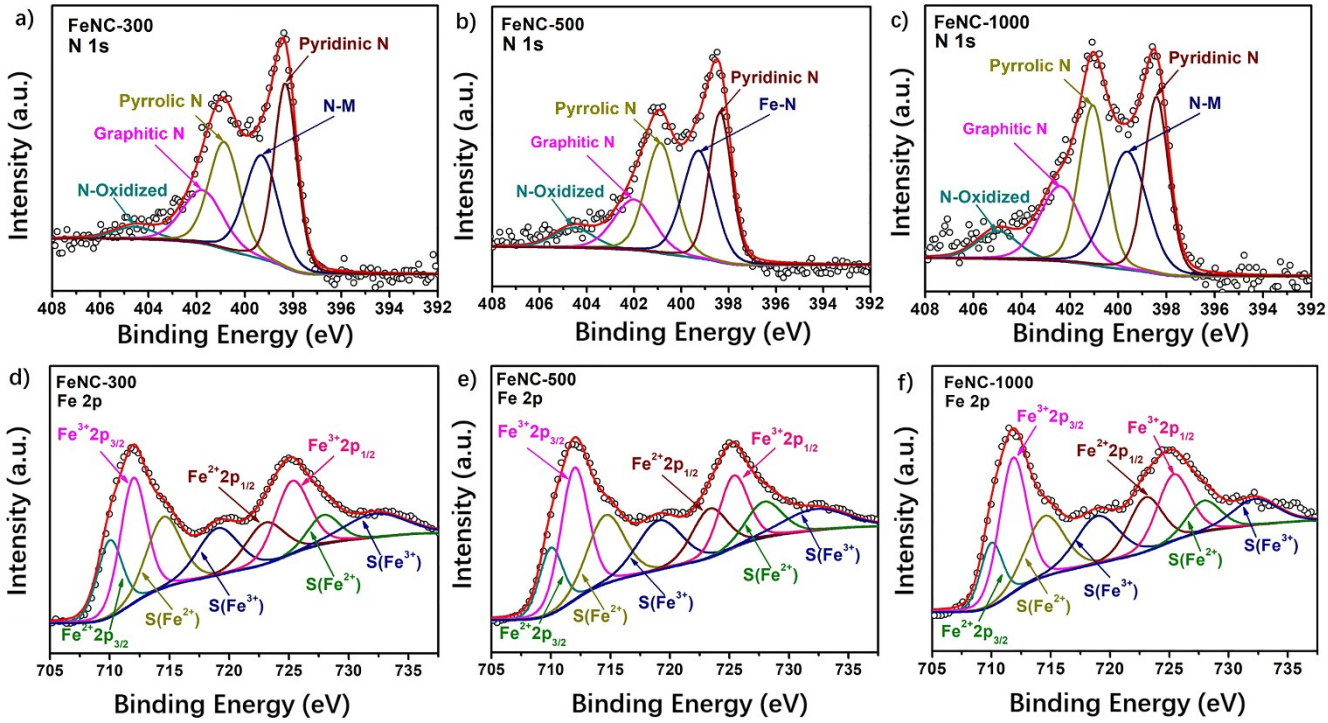

Figure S7. XPS spectra of N 1s for a) FeNC-300, b) FeNC-500 and c) FeNC-1000 catalysts, and Fe 2p for c) FeNC-300, d) FeNC-500 and e) FeNC-1000 catalysts

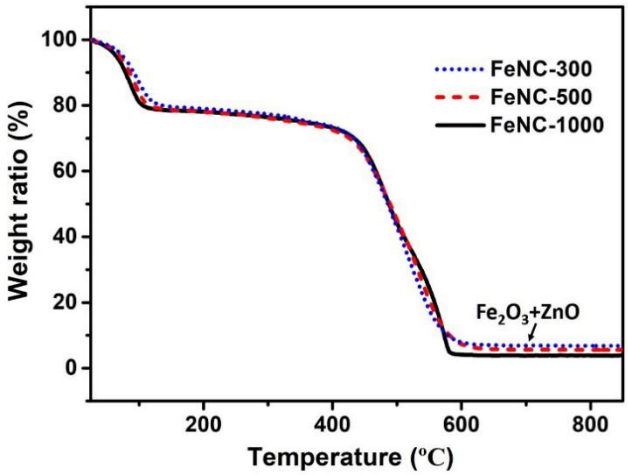

Figure S8. TG curves of FeNC-300/500/1000 catalysts measured in air.

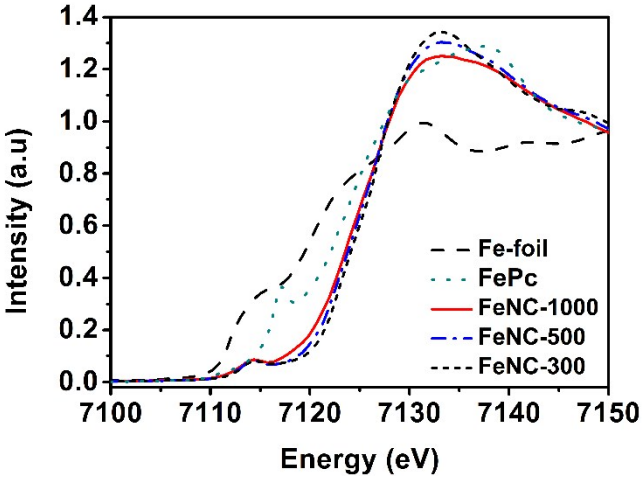

Figure S9. Normalized XANES spectra at Fe-K edge of FeNC-300/500/1000 and references.

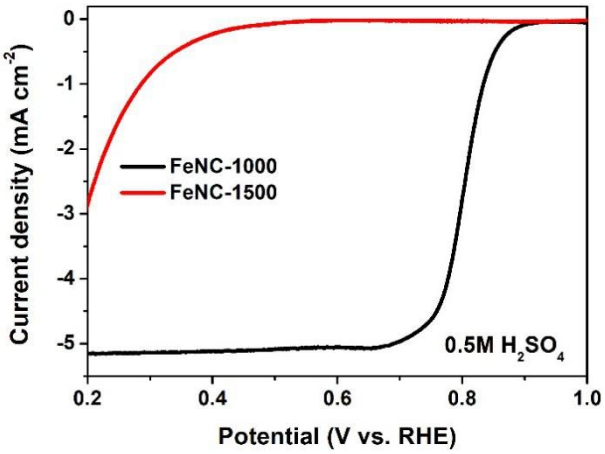

Figure S10. LSV curves of FeNC-1000 and FeNC-1500 in O_2 saturated 0.5 M H_2SO_4 by the RRDE test.

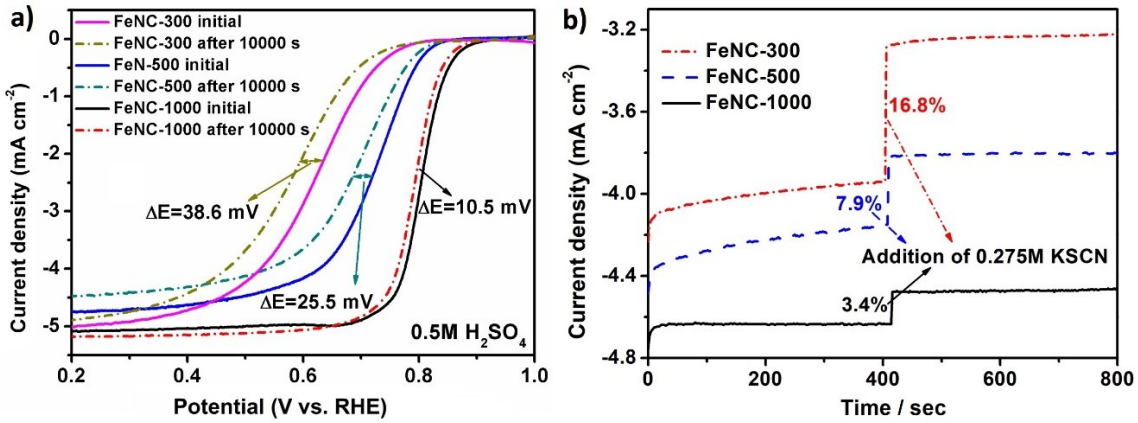

Figure S11. LSV curves of FeNC-300/500/1000 a) before and after durability tests, b) chronoamperometric curves of KSCN poisoning experiments tested at 0.50 V vs RHE. 0.375 M methanol was added at t = 400 s into the oxygen saturated 0.5 M H_2SO_4.

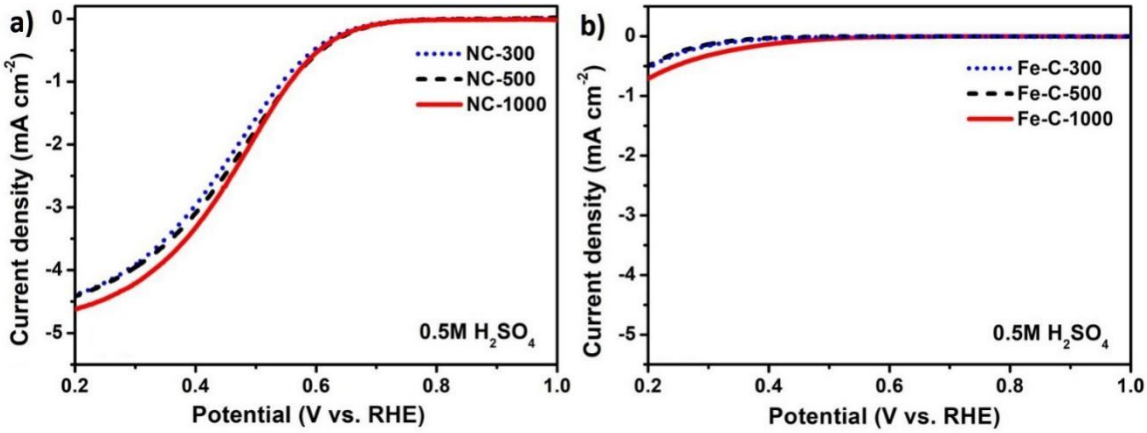

Figure S12. LSV curves of a) N/C-300/500/1000, b) Fe-C-/300/500/1000 in O_2 saturated 0.5 M H_2SO_4 by RRDE tests.

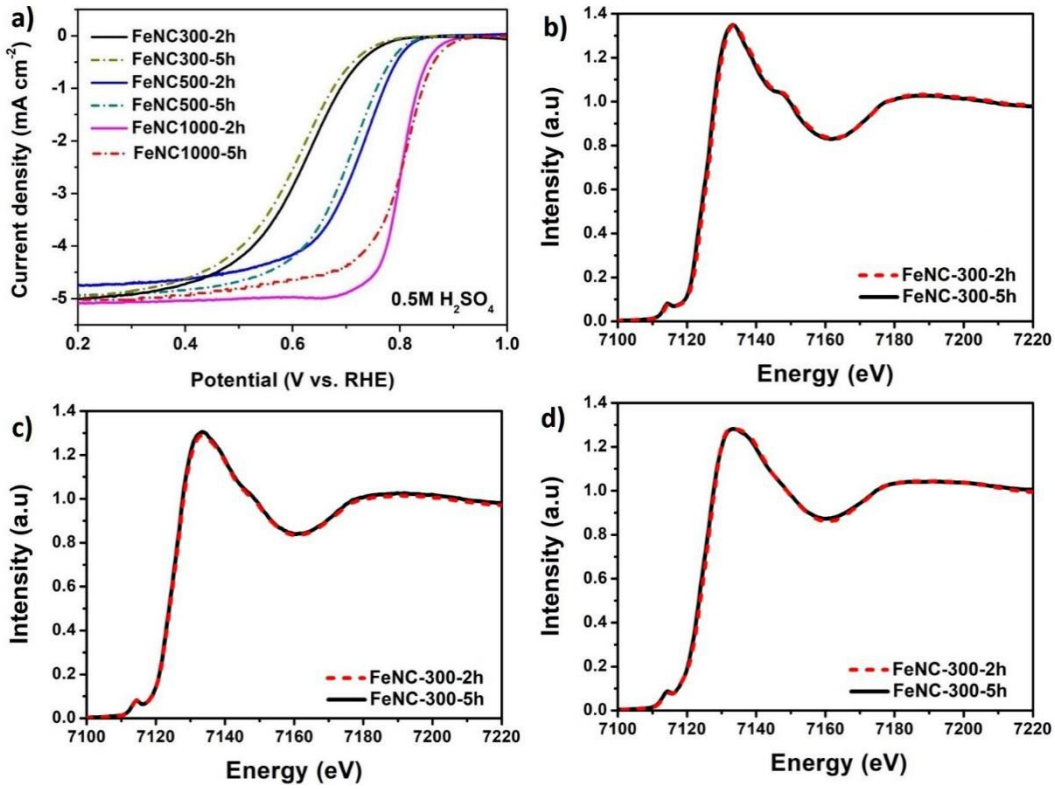

Figure S13. Comparison of FeNC-300/500/1000 prepared by 2 and 5 h pyrolysis. a) LSV curves measured in oxygen saturated 0.5 M H_2SO_4, b~d) XANES spectra at Fe-K edge.

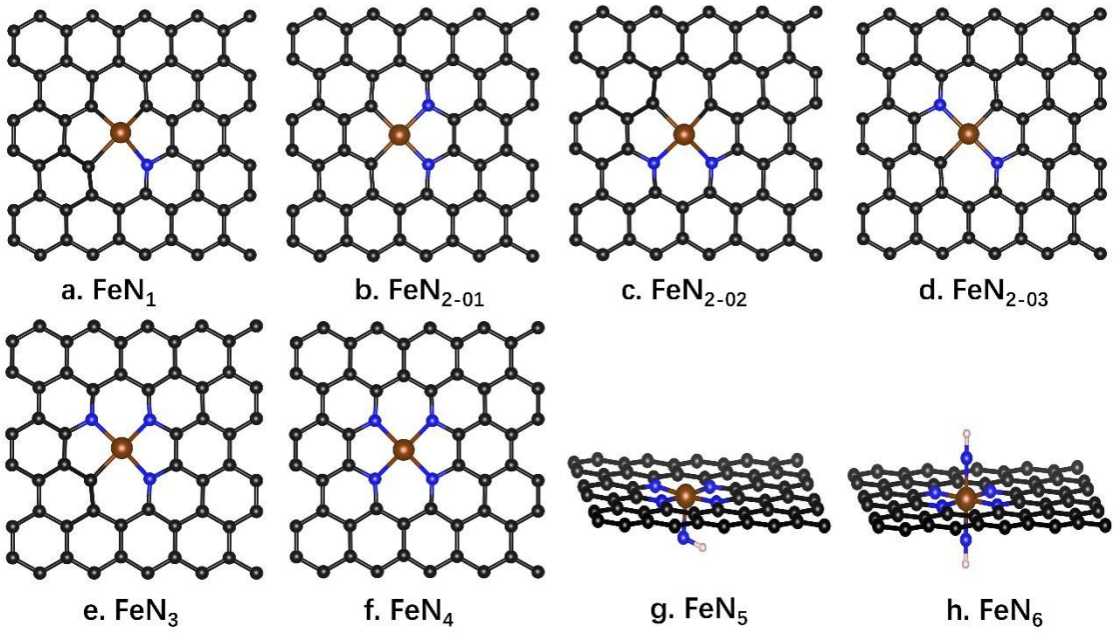

Figure S14. Atomic structures of FeN_1~FeN_6. Black, brown, white and blue balls represent C, Fe, H and N atoms respectively.

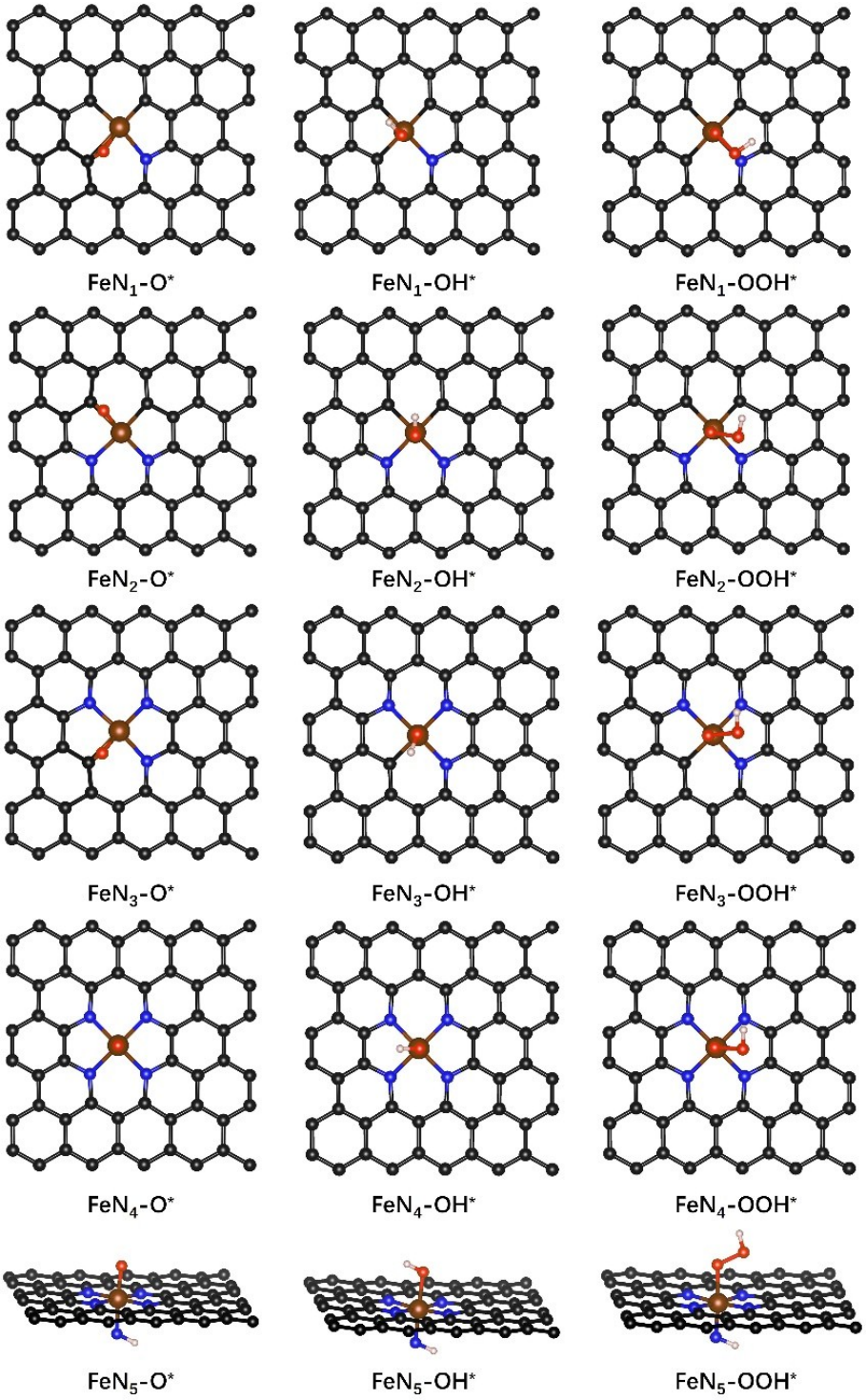

Figure S15. The most stable adsorption configurations of O, OH and OOH on FeN_x (x=1~5). Brown, blue, black, red and pink balls represent Fe, N, C, O and H atoms, respectively.

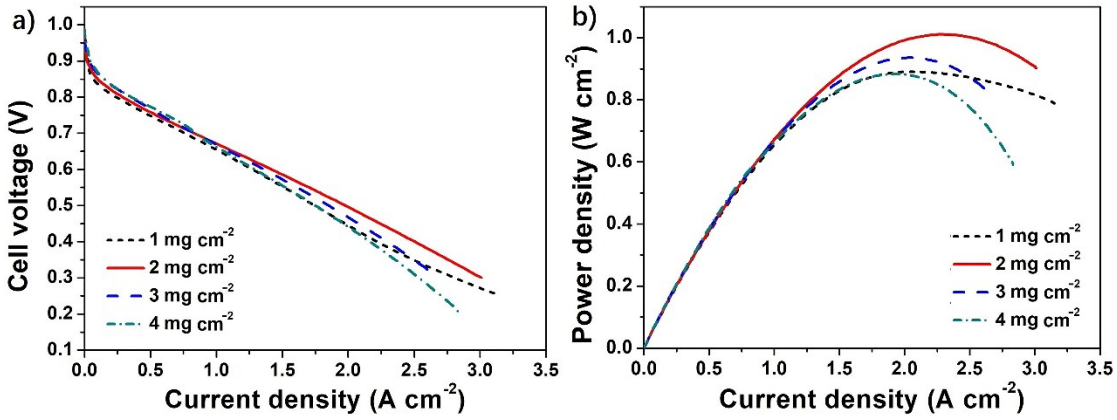

Figure S16. PEMFC a) polarization curves and b) power density curves of FeNC-1000 with the indicated loadings on cathode. (The fuel cell operation condition: 80 °C, 100% humidified H_2 and O_2 with flow rates of 200 and 240 mL min^{-1}, respectively. The gauge pressures of H_2 and O_2 are 22 psig.)

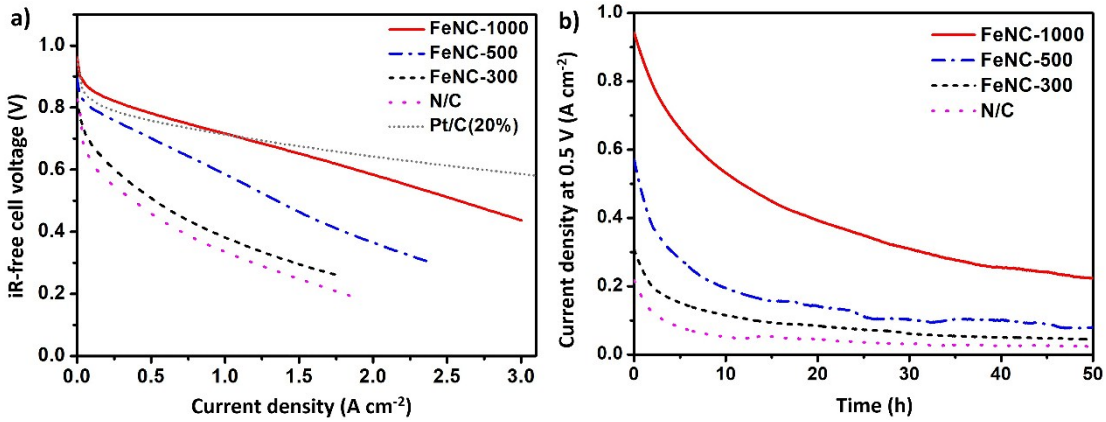

Figure S17. a) Internal resistance compensated polarization curves of FeNC-300/500/1000 and Pt/C(20 wt%). b) Durability tests in the fuel cell of FeNC-300/500/1000 in the initial 50 h measured at a constant voltage of 0.5 V at 80 °C. H_2 and O_2 flow rates are 200 and 240 mL min^{-1}, respectively.

Table S1. BET surface areas of the indicated materials.

Sample	ZIF-8	N/C	Fe@N/C	FeNC-300	FeNC-500	FeNC-1000
BET surface area (m^2 g^{-1})	1358	885	799	948	1054	1188

Table S2. Fe and Zn contents in the catalysts obtained by ICP measurements.

Sample	Fe (wt.%)	Zn (wt.%)
FeNC-300	0.25	0.86
FeNC-500	0.20	0.77
FeNC-1000	0.22	0.45

Table S3. C, O, Fe and N contents and the proportion of different types of nitrogen in FeNC-300/500/1000 obtained by XPS measurements.

Sample	FeNC-300	FeNC-500	FeNC-1000
C 1s (wt%)	81.89	81.68	82.84
O 1s (wt%)	6.84	6.92	7.22
Fe 2p (wt%)	3.77	3.83	3.91
N 1s (wt%)	7.89	7.76	5.93
N-oxidized/%	2.57	2.2	1.12
Graphitic N/%	7.98	9.01	11.43
Pyrrolic N/%	24.64	22.28	23.78
Fe-N/%	22.26	29.95	33.66
Pyridinic N/%	36.38	30.43	24.7

Table S4. Fitting results of Fe K-edge FT-EXAFS curves.

Sample	Path	*N*	*R*(Å)	σ^2(Å^2)	ΔE_0 (eV)	S_0^2	*R* factor
FeNC-300	Fe-C	3.1	1.96	0.0026	-7.02	0.92	0.0032
	Fe-N	1.0	2.00	0.0008			
	Fe-C	4.0	2.56	0.0042			
	Fe-C	4.1	2.69	0.0009			
	Fe-C	2.4	3.45	0.0002			
FeN-500	Fe-C	1.0	1.80	0.0006	2.74	0.92	0.0003
	Fe-N	2.8	2.03	0.0017			
	Fe-C	4.0	2.86	0.0181			
	Fe-C	3.8	3.04	0.0010			
	Fe-C	2.0	3.38	0.0042			
FeN-1000	Fe-N	4.0	1.92	0.0074	-3.67	0.92	0.0021
	Fe-C	3.9	2.61	0.0069			
	Fe-C	4.2	2.87	0.0066			
	Fe-C	2.3	3.43	0.0010			

N is coordination number, *R* is the distance between absorber and backscatter atoms, σ_2 is Debye-Waller factor to account for both thermal and structural disorders, ΔE_0 is inner potential correction; *R* factor indicates the goodness of the fit. Error bounds (accuracies) that characterize the structural parameters obtained by EXAFS spectroscopy were estimated as *N* ± 20%; *R* ± 1%; σ_2 ± 20%; ΔE_0 ± 20%. S_0^2 was fixed to 0.92 as determined from Fe foil fitting.

Table S5. ORR activities of Fe-N-C single atom catalysts with FeN_4 active sites.

Sample	Electrolyte	E_{onset} (V)	$E_{1/2}$ (V vs RHE)	Ref.
FeNC-1000	0.5 M H_2SO_4/0.1 M KOH	0.89/0.99	0.80/0.90	This Work
SA-Fe-N nanosheets	0.5 M H_2SO_4	0.94	0.81	[14]
(CM+PANI)-Fe-C	0.5 M H_2SO_4,	0.92*	0.80 V	[15]
FeN4/GN-2.7	1M NaOH	0.98*	0.91*	[16]
Fe-ISAs/CN	0.1 M KOH	0.99	0.9	[17]
FePhenMOF–ArNH3	0.1 M $HClO_4$	0.98	0.78	[18]
Fe2-Z8-C	0.5 M H_2SO_4/0.1 M KOH	0.90/0.99	0.81/0.87	[19]
Fe-N-C-950	0.1 M $HClO_4$	0.92	0.78	[20]
Fe-ZIF	0.5 M H_2SO_4	0.92*	0.85/0.88	[21]
SA-Fe/NG	0.5 M H_2SO_4	0.9	0.8	[22]
FeSAs/PTF-600	0.1 M $HClO_4$/0.1 M KOH	0.89/1.01	0.77*/0.87	[23]

*These values are not directly given in the papers. They were obtained by digging the polarization curves.

Table S6. Formation energies (eV) and ORR overpotentials (V vs RHE) of FeN_x (x=1~6) active sites calculated by DFT.

Active site	FeN_1	$FeN_{2\text{-}01}$	$FeN_{2\text{-}02}$	$FeN_{2\text{-}03}$	FeN_3	FeN_4	FeN_5	FeN_6
E_f	-1.24	-2.51	-2.75	-2.37	-3.82	-5.10	-4.09	-0.95
η^{ORR}	1.04	/	0.79	/	0.75	0.51	1.17	/

Table S7. Adsorption free energies of O, OH and OOH (eV) on FeN_x (x=1~5) sites.

Active site	ΔG_O^*	ΔG_{OH}^*	ΔG_{OOH}^*
FeN_1	0.65	0.46	3.70
FeN_2	1.20	0.44	3.93
FeN_3	1.21	0.48	3.94
FeN_4	1.48	0.77	3.89
FeN_5	3.01	1.70	4.85

Table S8. Adsorption energies of gaseous H_2O (eV) on FeNx (x=1~5) sites.

Active Site	FeN_1	$FeN_{2\text{-}6}$	FeN_3	FeN_4	FeN_5
E_{ads}	-0.33	-0.34	-0.28	-0.23	-0.04
Bond Length / Å	2.223	2.290	2.304	2.379	3.196

Table S9. Reaction free energies (eV) of elementary step for ORR at U_{RHE} = 0 V on FeN_x (x=1~5) active sites.

Active site	ΔG_1	ΔG_2	ΔG_3	ΔG_4
FeN_1	-1.22	-3.05	-0.19	-0.46
FeN_2	-0.99	-2.73	-0.75	-0.44
FeN_3	-0.97	-2.75	-0.72	-0.48
FeN_4	-1.03	-2.40	-0.72	-0.77
FeN_5	-0.06	-1.85	-1.31	-1.70

Table S10. $T \times S$ values (the entropy multiplied by T, T = 298.15 K,) and zero-point energy (*ZEP*) that are used to correct the free energy of reactants, products, and intermediate species adsorbed on FeN_x (x=1~5) active sites.

Species	$T\times S$ (eV)	*ZEP* (eV)
O^*	0	0.10/0.07
OH^*	0	0.34
OOH^*	0	0.43
O_2	0.64	0.10
H_2	0.41	0.27
H_2O	0.67	0.56

***** The *ZPE* values of O^* on the bridge site and top side are 0.10 and 0.07 eV respectively. The *ZPE* values of OH^* and OOH^* are averaged over all single atom catalyst systems because they have very close value.

4. References:

1 D. Zhang, W. Chen, Z. Li, Y. Chen, L. Zheng, Y. Gong, Q. Li, R. Shen, Y. Han, W. C. Cheong, L. Gu and Y. Li, *Chem. Commun.*, 2018, **54**, 4274-4277.

2 M. Newville, *J.Synchrotron Radiat.*, 2001, **8**, 322-324.

3 H. Xu, D. Cheng, D. Cao and X. C. Zeng, *Nat. Catal.*, 2018, **1**, 339-348.

4 X. Zhang, Z. Yang, Z. Lu and W. Wang, *Carbon*, 2018, **130**, 112-119.

5 C. Zhao, X. Dai, T. Yao, W. Chen, X. Wang, J. Wang, J. Yang, S. Wei, Y. Wu and Y. Li, *J. Am. Chem. Soc.*, 2017, **139**, 8078-8081.

6 G. Kresse and J. Furthmiiller, *Comput. Mater. Sci.* , 1996, **6**, 15-50.

7 G. Kresse and J. Furthmiiller, *Phys. Rev. B*, 1996, **54**, 11169-11186

8 G. Kresse and D. Joubert, *Phys. Rev. B*, 1999, **59**, 1758-1775.

9 J. P. Perdew, K. Burke and M. Ernzerhof, *Phys. Rev. Lett.* , 1996, **77**, 3865-3868.

10 I. C. Man, H.-Y. Su, F. Calle-Vallejo, H. A. Hansen, J. I. Martínez, N. G. Inoglu, J. Kitchin, T. F. Jaramillo, J. K. Nørskov and J. Rossmeisl, *ChemCatChem*, 2011, **3**, 1159-1165.

11 J. K. Nørskov, J. Rossmeisl, A. Logadottir and L. L, *J. Phys. Chem. B*, 2004, **108**, 17886–17892.

12 J. K. Nørskov, J. Rossmeisl, A. Logadottir and L. L, *J. Phys. Chem. B*, 2004, **108**, 17886-17892.

13 F. Calle-Vallejo, J. I. Martinez and J. Rossmeisl, *Phys. Chem. Chem. Phys.*, 2011, **13**, 15639-15643.

14 Z. Miao, X. Wang, M.-C. Tsai, Q. Jin, J. Liang, F. Ma, T. Wang, S. Zheng, B.-J. Hwang, Y. Huang, S. Guo and Q. Li, *Adv. Energy. Mater.*, 2018, **8**, 1801226.

15 H. T. Chung, D. A. Cullen, D. Higgins, B. T. Sneed, E. F. Holby, K. L. More and P. Zelenay, *Science*, 2017, **357**, 479–484.

16 X. Chen, L. Yu, S. Wang, D. Deng and X. Bao, *Nano Energy*, 2017, **32**, 353-358.

17 Y. Chen, S. Ji, Y. Wang, J. Dong, W. Chen, Z. Li, R. Shen, L. Zheng, Z. Zhuang, D. Wang and Y. Li, *Angew. Chem. Int. Ed.*, 2017, **56**, 6937-6941.

18 J. Li, S. Ghoshal, W. Liang, M.-T. Sougrati, F. Jaouen, B. Halevi, S. McKinney, G. McCool, C. Ma, X. Yuan, Z.-F. Ma, S. Mukerjee and Q. Jia, *Energy Environ. Sci.*, 2016, **9**, 2418-2432.

19 Q. Liu, X. Liu, L. Zheng and J. Shui, *Angew. Chem. Int. Edit.*, 2018, **57**, 1204-1208.

20 M. Xiao, J. Zhu, L. Ma, Z. Jin, J. Ge, X. Deng, Y. Hou, Q. He, J. Li, Q. Jia, S. Mukerjee, R. Yang, Z. Jiang, D. Su, C. Liu and W. Xing, *ACS Catal.*, 2018, **8**, 2824-2832.

21 H. Zhang, S. Hwang, M. Wang, Z. Feng, S. Karakalos, L. Luo, Z. Qiao, X. Xie, C. Wang, D. Su, Y. Shao and G. Wu, *J. Am. Chem. Soc.*, 2017, **139**, 14143-14149.

22 L. Yang, D. Cheng, H. Xu, X. Zeng, X. Wan, J. Shui, Z. Xiang and D. Cao, *Proc. Natl. Acad. Sci.*, 2018, **115**, 6626-6631.

23 J. Yi, R. Xu, Q. Wu, T. Zhang, K.-T. Zang, J. Luo, Y.-L. Liang, Y.-B. Huang and R. Cao, *ACS Energy Lett.*, 2018, **3**, 883-889.